Temperature-Dependent Kinetics of the Gas-Phase Reactions of OH with Cl₂, CH₄, and C₃H₈

Mikhail G. Bryukov,[†] Vadim D. Knyazev,[‡] Slawomir M. Lomnicki,[†] Cheri A. McFerrin,[†] and Barry Dellinger*,[†]

Chemistry Department, Louisiana State University, Baton Rouge, Louisiana 70803, and Research Center for Chemical Kinetics, Department of Chemistry, The Catholic University of America, Washington, D.C. 20064

The reactions of OH with molecular chlorine (reaction 1), methane (reaction 2), and propane (reaction 3) have been studied experimentally using a pulsed laser photolysis/pulsed-laser-induced fluorescence technique over wide ranges of temperatures (297−826, 298−1009, and 296−908 K, respectively) and at pressures between 6.68 and 24.15 kPa. The rate coefficients obtained for reactions 1−3 demonstrate no dependence on pressure and exhibit positive temperature dependences that can be represented with modified three-parameter Arrhenius expressions within their corresponding experimental temperature ranges: $k_1 = 3.59 \times 10^{-16} \, T^{1.35} \exp(-745 \, \text{K}/T)$ cm³ molecule⁻¹ s⁻¹, $k_2 = 3.82 \times 10^{-19} \, T^{2.38} \exp(-1136 \, \text{K}/T)$ cm³ molecule⁻¹ s⁻¹, and $k_3 = 6.64 \times 10^{-16} \, T^{1.46} \exp(-271 \, \text{K}/T)$ cm³ molecule⁻¹ s⁻¹. For the OH + Cl₂ reaction, the potential energy surface has been studied using quantum chemical methods, and a transition-state theory model has been developed on the basis of calculations and experimental data. Model predictions suggest OH + Cl₂ → HOCl + Cl as the main channel of this reaction. The model results in the expression $k_1 = 1.35 \times 10^{-16} \, T^{1.50} \exp(-723 \, \text{K}/T)$ cm³ molecule⁻¹ s⁻¹ for the temperature dependence of the reaction 1 rate coefficient extrapolation outside the experimental range to low temperatures down to 200 K and to high temperatures up to 3000 K. A temperature dependence of the rate coefficient of the HOCl + Cl → OH + Cl₂ reaction has been derived on the basis of the experimental data, modeling, and thermochemical information.

I. Introduction

The hydroxyl radical plays a key role in the chemistry of combustion and atmospheric processes. Numerical simulation of the complicated chemistry of these phenomena requires a large database of accurately determined reaction rate coefficients in a wide range of temperatures and pressures. This article is devoted to the experimental and theoretical temperature-dependent kinetic investigation of the gas-phase reaction of the hydroxyl radical with molecular chlorine

$$OH + Cl_2 \rightarrow \text{products} \qquad (1)$$

over a wide temperature range.

Molecular chlorine is produced in large quantities. According to a conservative estimate reported by the U.S. Environmental Protection Agency, the annual production of molecular chlorine is about 10⁷ metric tons just in the United States. The largest users of molecular chlorine are companies that manufacture ethylene dichloride and other chlorinated solvents, poly(vinyl chloride) resins, chloroflurocarbons, and propylene oxide. As a result of this activity, large quantities of wastes with chlorine-containing compounds are incinerated, subject to thermal degradation, or accidental fires. For the incineration of industrial wastes to be more efficient and less hazardous, it is necessary to understand all aspects of this process. This understanding is especially important for chlorine-containing compounds, whose

burning has the potential to generate products such as phosgene, molecular chlorine, polychlorinated dibenzodioxins, polychlorinated dibenzofurans, and polychlorinated biphenyls,[1−3] which are more hazardous than the originally incinerated waste. Accurate kinetic modeling of these processes is essential for understanding their mechanisms and for use of these mechanisms as tools of prediction and control.

Reaction 1 plays a significant role in the formation of the hazardous emissions from combustion of chlorine-containing compounds[1−4] as, for example, it may be important in the control of the HCl to Cl₂ ratio. Molecular chlorine is an effective chlorinating agent and a powerful oxidant, whereas the larger bond dissociation energy in HCl can result in significant sequestration of chlorine. In addition, Cl₂ is difficult to scrub from the flue gas, because of its relatively low water solubility. Therefore, the emissions of Cl₂ should be controlled and minimized during the combustion process.[2] Despite reaction 1 being potentially important in these processes, the rate coefficient of this reaction has not been studied at high temperatures.

Reaction 1 has been previously studied at low temperatures,[5−9] and the results of these studies are in agreement with each other within reported experimental errors. The importance of this reaction for atmospheric chemistry is described in the work of Gilles et al.[9] The current work represents the first experimental study of reaction 1 carried out at high temperatures in the range from 297 K (to compare with the earlier studies) to 826 K, which is relevant to combustion and thermal processes.

To accurately determine the rate coefficients of hydroxyl radical reactions, experiments must be performed with suf-

* To whom correspondence should be addressed. E-mail: BarryD@LSU.edu.
† Louisiana State University.
‡ The Catholic University of America.

ficiently low initial concentrations of hydroxyl radicals, thus ensuring the absence of any complications due to possible fast secondary reactions. For this purpose, we have constructed a pulsed laser photolysis/pulsed-laser-induced fluorescence apparatus combined with a heatable, slow-flow reactor. This technique has excellent sensitivity to hydroxyl radicals (vide infra), which allows one to perform OH reaction rate measurements with the necessary low initial OH concentrations. Two reactions whose rate coefficients are relatively well-established (see refs 10−16 and references therein), reactions 2 and 3, were

$$OH + CH_4 \rightarrow H_2O + CH_3 \ (298-1009 \ K) \qquad (2)$$

$$OH + C_3H_8 \rightarrow products \ (296-908 \ K) \qquad (3)$$
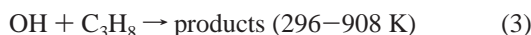
also studied in order to validate the experimental apparatus used here for the first time after its construction. (Numbers in parentheses indicate the experimental temperature ranges of the current study.)

II. Experimental Section

II. A. Experimental Apparatus. A schematic of the experimental apparatus and the optical test cell (reactor) are depicted in Figure 1a and b, respectively. This pulsed laser photolysis/pulsed-laser-induced fluorescence apparatus is similar to the one described in ref 17. An ArF excimer laser (LAMBDA PHYSIK: COMPEX 102) and an Nd:YAG (Quanta-Ray: DCR-2a) pumped, frequency doubled, tunable pulsed dye laser (Quanta-Ray: PDL-3) were employed to generate the pump and probe beams, respectively.

Pulsed, unfocused 193-nm radiation (10 Hz) from the excimer laser was directed through two iris diaphragms, D_1 and D_2, and a fluorescence-free UV fused silica window, W_1, into a quartz tubular six-way cross that served as the base of the optical test cell. The pump (photolysis) beam was responsible for creation of the hydroxyl radicals. In most experiments, hydroxyl radicals were formed following the 193-nm laser photolysis of nitrous oxide producing excited $O(^1D)$ atoms followed by rapid reaction with molecules of water[14,17,18]

$$N_2O + h\nu(193 \ nm) \rightarrow N_2 + O(^1D) \qquad (4)$$

$$O(^1D) + H_2O \rightarrow 2OH \qquad (5)$$
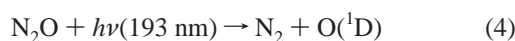
When CH_4 or C_3H_8 was present in the reaction mixture, OH could potentially be produced via reactions of $O(^1D)$ with one of these species that can occur simultaneously with reaction 5. In selected experiments, we produced hydroxyl radicals by the 193-nm laser photolysis dissociation of H_2O only ($[N_2O] = 0$, also see ref 11) to avoid possible effects from the thermal decomposition of N_2O at high reaction temperatures and to verify that the results were independent of the method of OH generation.

Pulsed, unfocused radiation (10 Hz) from the probe laser was directed using two flat laser (UV enhanced, aluminum coated) mirrors, M_1 and M_2, and passed through two iris diaphragms, D_3 and D_4, and a fluorescence-free UV fused silica window, W_2, placed at a Brewster angle into the detection zone of the optical test cell.

After the pulse of the excimer laser, the pulse of the probe laser induced excitation of hydroxyl radicals. OH was excited at approximately 282 nm via the $A^2\Sigma^+-X^2\Pi$ (1−0) transition followed by observation of fluorescence from the (1−1) and (0−0) bands at 308−316 nm (see, for example, refs 19, 20). The fluorescent radiation was monitored with a photomultiplier

tube (Electron Tubes Limited: P10N-01W) using a UV band-pass filter (308 nm peak transmission) to reduce scattered light. The signal from the photomultiplier was amplified (Electron Tubes Limited: transimpedance amplifier A1) and then recorded by an oscilloscope (Tektronix: TDS 714L digitizing oscilloscope). A signal induced by the probe beam in a photodiode, Ph_2, triggered the oscilloscope. The oscilloscope allows one to obtain the integrated voltage averaged for a desired number of pulses (typically 150) of the lasers at single time delay. The value, S_t, received from the integration of the average voltage signal is a sum of two components: the integral from the average laser-induced fluorescence signal of OH radicals, S_{OH}, (this term is proportional to the absolute concentration of OH) and the integral from the average scattered light signal, S_{sc}. The average integrated voltage for the scattered light was measured directly in the absence of OH radicals. For this measurement, the photolysis laser was not triggered during the accumulation of the scattered light signal. Kinetic information was obtained by varying the time delay between pulses of the pump and the probe lasers in the desired time interval. We used a pulse generator (Stanford Research System: DG535 digital delay/pulse generator) to trigger the excimer laser and the Nd:YAG laser with different time delays.

We developed software using *Visual Basic 6.0* to obtain the temporal profiles automatically. Kinetic data (S_t values with corresponding reaction time delays t and S_{sc} value) were collected in the computer for the subsequent data processing. S_{sc} was subtracted from S_t measured at different reaction time delays and one fixed concentration of molecular substrate to obtain a relative OH concentration temporal profile $S_{OH} = S_t - S_{sc}$. The systematic uncertainty in the experimentally obtained S_{OH} values (the deviation from linearity) was defined using characteristics of the accuracy stated by the manufacturers for the photomultiplier, amplifier, and oscilloscope. The maximum of the systematic deviation of the OH concentration detection system from linearity has been estimated as 3.0%.

Helium was used as the carrier gas in all experiments presented in this article. We utilized four separately controlled gas flows to prepare a reaction gas mixture. Three of them were the main flow of helium, the flow of nitrous oxide diluted with helium (200−1000 times), and the flow of helium containing water vapor. Water vapor was added to the third flow of helium by bubbling helium though water at controlled pressure and temperature in a thermostabilized saturator maintained at a temperature ~2 K below ambient temperature. We employed three calibrated mass-flow controllers (SIERRA Instruments, Inc., model 810C) with appropriate flow ranges to establish the values of the three gas flows and maintain their stability during the performance of the experiments. At selected times during the experiments, we controlled values of these three flows by measuring rates of pressure increases in the calibrated volumes located upstream from the gas inlet of the optical test cell. These pressure measurements were performed with capacitance manometers (MKS Instruments, model 626A13TAE, range 1000 Torr or model 622A12TAD, range 100 Torr). The fourth flow of undiluted molecular substrate was manually regulated by a metering valve (Swagelok, type SS-SS4). This flow was also determined by measuring the rate of the pressure increase in the calibrated volume before and after obtaining each OH temporal profile. A mean value of these two flow measurements was taken to calculate molecular substrate concentration in the reaction zone. The independence of the measured flows on the surface-to-volume ratio of the calibrated volume was verified

to ensure the absence of interference from heterogeneous absorption and desorption processes on the walls of this volume. All flows were premixed and directed though the reactor. The total flow rate ranged between 5.0 and 25 STP cm^3 s^{-1}. The value of the total flow was set depending on total pressure and temperature in the reaction zone to ensure slow-flow conditions, such that each photolysis pulse-initiated reaction within a locally fresh gas mixture, eliminating potential complications that might result from accumulation of the photolysis or reaction products. The composite flow conditioned the reactor for several minutes prior to data collection, thereby minimizing any effects due to reactant adsorption on the reactor walls and stabilizing the established experimental conditions. The maximum systematic uncertainty in the ratio of the measured molecular substrate flow rate to the total flow rate of the reaction gas mixture has been evaluated as 1.5% of this ratio value.

Pressure in the reactor was monitored with the capacitance manometers described earlier. A pressure measurement inlet was located (see Figure 1b) at the main axis, ~15 mm downstream of the photolysis zone in the quartz tubular six-way cross. The maximum systematic uncertainty in the reaction pressure, P, was evaluated as 0.7% of this pressure value based on the finite accuracies stated by the manufacturers for the devices used in pressure monitoring.

The reactor was resistively heated. A heater, thermoinsulator, two temperature controllers (series CN77000), and Chromel-Alumel thermocouples were supplied by OMEGA Engineering, Inc. We employed two Chromel-Alumel thermocouples to control the temperature within the heated zone. The first 0.813-mm diameter thermocouple was fixed at the main axis, ~5 mm downstream from the photolysis zone of the quartz tubular six-way cross (see Figure 1b). The temperature field inside the heated zone with the desired temperature in the detection zone (reaction temperature) was stabilized by using this thermocouple installed with the temperature controller connected to the reactor heater. The temperature field inside the heated zone was measured (calibrated) with the second movable 0.508-mm diameter Chromel-Alumel thermocouple and referenced to the readout of the first thermocouple. The maximum total uncertainty in the measurements of the reaction temperatures, T, did not exceed 0.5% of T and was considered as the systematic source of the experimental errors because of its behavior revealed during the calibration and experiments.

The molecular concentration of each reactant in the reaction zone was calculated by means of the multiplication of three values: the total concentration in the reaction zone derived from measured pressure and temperature using the ideal gas law, the molecular partial concentration in the flow carrying the reactant, and the value of the ratio of the flow carrying the reactant to the total gas flow rate. Typical reaction mixtures used in these experiments consisted of the following molecular concentrations: N_2O, $3.6 \times 10^{12} - 1.5 \times 10^{14}$ or 0.0; H_2O, $4.0 \times 10^{14} - 2.1 \times 10^{15}$; He, $5.06 \times 10^{17} - 3.99 \times 10^{18}$; Cl_2, $0.0 - 5.07 \times 10^{15}$; CH_4, $0.0 - 3.89 \times 10^{16}$; C_3H_8, $0.0 - 3.49 \times 10^{15}$ in units of molecule cm^{-3}.

The chemicals utilized in this study had the following stated minimum purities (and were supplied by): He, 99.999% (The BOC Group, Inc.); Cl_2, 99.999% (Matheson Tri-Gas, Inc.); CH_4, 99.999% (Matheson Tri-Gas); C_3H_8, 99.993% (Matheson Tri-Gas); N_2O, 9.98% mixture of 99.99% purity in 99.999% He (The BOC Group); H_2O, A.C.S. reagent grade (Aldrich). Analyses of Cl_2, CH_4, and C_3H_8 samples showed only trace levels of impurities, and these small concentrations had a negligible effect on the observed OH decay rates.
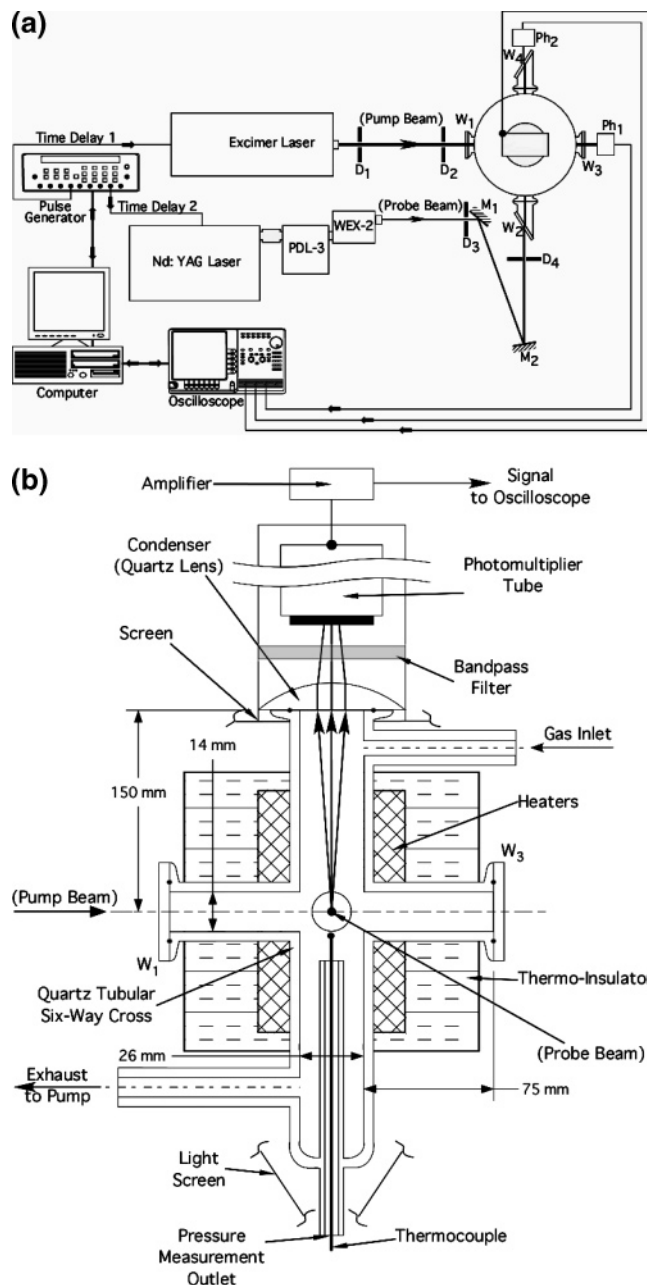

(a)

(b)

Figure 1. a. Schematic drawing of the experimental apparatus. b. Two-dimensional schematic drawing of the optical test cell (reactor). The probe beam is perpendicular to the plane of the figure and intersects the pump (photolysis) laser beam in the center of the reactor.

II. B. Reaction Rate Measurements and Data Processing. All experiments to measure the rate coefficients of reactions 1−3 were conducted under pseudo-first-order kinetic conditions with a large excess of molecular substrate $[Cl_2]$, $[CH_4]$, $[C_3H_8]$ ≫ $[OH]_0$. An estimated initial concentration of OH radicals in the detection zone was in the range $1.0 \times 10^{10} - 3.0 \times 10^{11}$ molecule cm^{-3}, at least two orders of magnitude smaller than the lowest molecular substrate concentration. We estimated OH initial concentrations on the basis of a photolysis laser pulse intensity measured as it entered the reactor, published UV absorption coefficients of N_2O,[21] our own experimental evaluation of the absorption cross section of N_2O at 193 nm performed at different temperatures, and on the assumption that the maximum possible total yield of OH formation was equal to 2.0 per absorption of one photon by N_2O in the presence of H_2O. The initial OH concentrations produced from the direct
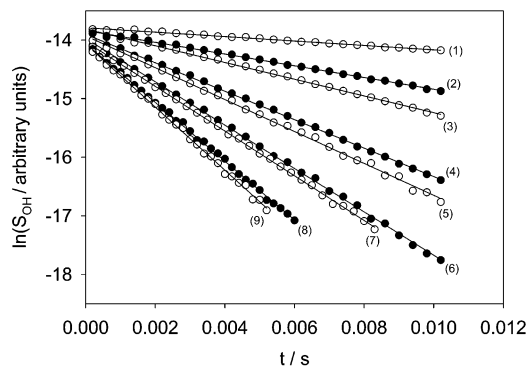
Figure 2. Examples of relative OH temporal profiles obtained under the following conditions: helium buffer gas, total pressure $P = 20.10$ kPa (150.8 Torr), temperature $T = 365$ K, $[N_2O] = 3.8 \times 10^{13}$ cm^{-3}, $[H_2O] = 1.59 \times 10^{15}$; $[MS] = [Cl_2] = 0$, 5.11×10^{14}, 9.09×10^{14}, 1.54×10^{15}, 1.76×10^{15}, 2.38×10^{15}, 2.52×10^{15}, 3.42×10^{15}, 3.75×10^{15} cm^{-3} for profiles 1–9, respectively.

photolysis of H_2O were estimated by comparing the S_{OH} values obtained in the presence of N_2O to those obtained in the absence of N_2O at different concentrations of H_2O and N_2O and temperatures. The values of the initial concentrations of OH radicals used in the experiments to determine the rate coefficients of reactions 1–3 (listed in Tables 1, 2) are somewhat overestimated and should be understood as upper limits to $[OH]_0$. Exact knowledge of the initial OH concentrations is not needed for the determination of rate coefficients, because the experiments were conducted under pseudo-first-order conditions. The evaluated detection sensitivity for OH radicals ranged from 1×10^8 to 5×10^8 molecule cm^{-3} depending on experimental conditions.

Examples of temporal profiles of the set of experiments are shown in Figure 2 as a plot of $\ln(S_{OH})$ versus t. The initial reaction time value, t_0, in all OH temporal profiles was not less than 0.2 ms. This time delay followed the photolysis of the reaction mixture and was sufficient for the completion of the reaction 5 and for rotational and vibrational equilibration of OH radicals to the Boltzmann distribution.[18,22]

We analyzed each set of experiments at first assuming first-order kinetic behavior of OH decay

$$\ln(S_{OH}) = \text{constant} - k't \tag{I}$$

where

$$k' = k_i[MS] + k_0 \tag{II}$$

is the effective first-order rate coefficient, k_i is the bimolecular rate coefficient of the reaction under study ($i = 1, 2, 3$), $[MS]$ ($[MS] = [Cl_2]$, $[CH_4]$, $[C_3H_8]$) is the molecular substrate concentration, and k_0 is the effective first-order rate coefficient of OH decay due to possible OH reactions with background impurities in the buffer gas and N_2O, H_2O precursors, OH diffusion, and flow out of the detection zone (OH background loss). The effective first-order rate coefficient values, k' values, were obtained from linear least-squares fits of the experimental values of $\ln(S_{OH})$ to eq I. (These least-squares fits and all next least-squares fits were performed with no weighting of the data points.) Examples of measured k' versus molecular substrate concentration dependences are presented in Figures 3 and 4a,b (for Cl_2, CH_4, and C_3H_8 substrates, respectively). We determined the bimolecular rate coefficient, k_i, from the slope of the least-squares straight line drawn through the k' versus $[MS]$ data points including the $(0, k_0)$ point, where k_0 was derived from
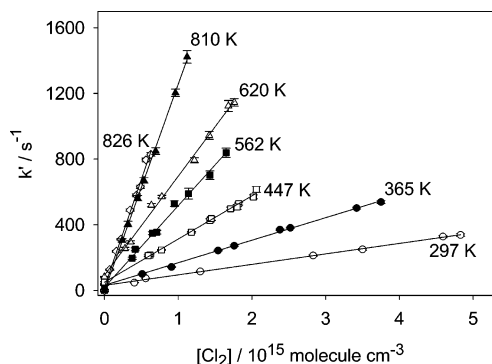

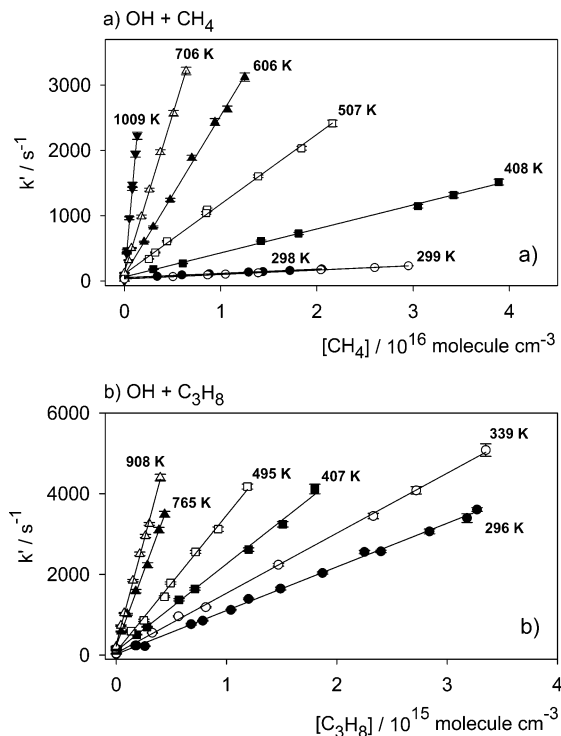**Figure 3.** Examples of experimentally obtained k' vs $[Cl_2]$ dependences.

Figure 4. Examples of experimentally obtained k' vs $[CH_4]$ (part a) and k' vs $[C_3H_8]$ (part b) dependences.

the OH temporal profile directly measured at zero concentration of the molecular substrate.

However, under some experimental conditions, the OH temporal profile detected at $[MS] = 0$ and then plotted in $[t, \ln(S_{OH})]$ coordinates displayed a reproducible positive curvature. By varying the reaction pressure, temperature, total flow rate, and diameter of the photolysis beam, we found that the appearance of this curvature was mainly caused by the process of the OH diffusion out of the detection zone. All sets of the experiments with such behavior of OH background loss were also treated by data processing that is similar to that described in refs 23–26. This method of data processing allows one to analyze and decrease the possible effect of the non-first-order kinetic behavior of the OH background loss on the measured k_i value. During the first stage of data processing, each OH temporal profile recorded in the presence of the molecular substrate was point-by-point divided into the common interval of time delays by the OH temporal profile recorded in the absence of molecular substrate, in order to obtain OH background loss-corrected temporal profiles. These background loss-corrected temporal profiles were then treated by data

10468   *J. Phys. Chem. A, Vol. 108, No. 47, 2004*

Bryukov et al.

TABLE 1: Conditions and Results of Experiments to Measure Rate Coefficients of the Reaction of Hydroxyl Radicals with Molecular Chlorine

no.[a]	T/K	P/kPa	$[Cl_2]$ range/ 10^{14} molecule cm^{-3}	I^b/mJ pulse^{-1} cm^{-2}	$[OH]_0$/10^{10} molecule cm^{-3}	$k_1{}^c$/10^{-14} molecule^{-1} cm^3 s^{-1}
1	297	13.41	4.84–50.7	13	30	6.25 ± 0.31
2	297	13.40	4.05–48.3	2.6	6.0	6.38 ± 0.21
3	330	6.70	4.58–41.7	12	19	9.25 ± 0.67
4	330	6.72	4.63–33.1	2.8	4.4	9.28 ± 0.26
5	365	20.10	5.11–37.5	11	9.6	13.72 ± 0.44
6	404	13.41	3.05–49.1	11	17	19.72 ± 0.33
7	404	13.40	3.11–19.1	2.6	4.0	19.00 ± 0.38
8	447	13.41	5.94–20.6	11	12	26.32 ± 0.96
9	447	13.41	5.93–20.7	2.6	2.8	25.2 ± 1.3
10	501	13.41	3.71–43.5	11	7.0	35.7 ± 1.7
11	501	13.42	3.21–20.2	11	7.3	36.9 ± 2.3
12	562	6.70	3.76–16.5	12	4.3	49.7 ± 3.0
13	562	6.70	3.79–16.3	12	4.3	50.7 ± 4.0
14	620	13.40	2.78–17.6	4.3	5.9	60.3 ± 2.6
15	620	13.39	3.18–16.8	12	16	59.0 ± 3.6
16	719	13.42	1.44–10.1	13	19	87.1 ± 4.0
17	719	13.42	1.43–10.7	2.6	3.8	87.7 ± 5.0
18	810	10.74	2.4–11.2	10	16	125.8 ± 2.5
19	810	10.74	2.39–11.1	2.1	3.4	124.7 ± 7.4
20*	825	10.73	1.19–5.68	13	3.8	131.0 ± 7.9
21*	825	21.46	3.79–10.9	13	7.6	121.5 ± 4.1
22*	826	13.39	0.71–6.3	12	4.4	131.3 ± 6.9

[a] Experiment number. $[N_2O] = 0$ was in experiments marked with *. [b] Photolysis laser intensity. [c] Error limits represent 2σ statistical uncertainties only. Maximum estimated systematic uncertainty is 5% of the rate coefficient value (see text).

processing described in the previous paragraph. The linear least-squares fit method with two floated parameters was applied in both stages to obtain $k' = k_i[MS]$ (in this case) and k_i values. The point with (0, 0) coordinates was always included in the data points set of the third stage. For the same set of experiments, the application of data processing with the background loss correction stage always yielded a lower value for k_i than the value obtained by applying the data processing without the background loss correction stage; however, the difference between these two values never exceeded 4% of their average value. Only in those cases where this difference was 1.0% or more of the k_i value, the k_i value obtained by the data processing with the background loss correction stage was taken as the result of its measurement for the subsequent consideration, instead of the k_i value obtained assuming first-order kinetic behavior of OH decay. Therefore, a systematic uncertainty in the experimentally obtained rate coefficients, caused by unaccounted-for deviation of OH background loss from the first-order kinetic behavior, was evaluated as 1% of k_i and taken into account in the evaluation of the systematic error of the measured bimolecular rate coefficients (vide infra).

II. C. Experimental Results. The kinetic study of the reactions of OH with Cl_2, CH_4, and C_3H_8 was performed over the temperature ranges of 297–826, 298–1009, and 296–908 K and at pressures between 6.7 and 21.46, 6.71 and 24.15, and 6.68 and 24.13 kPa, respectively. The initial concentration of OH radicals was varied by changing the photolysis laser intensity, the concentration of N_2O, and the concentration of H_2O. Conditions and results of experiments to determine the values of the rate coefficients of reactions 1–3 are presented in Tables 1 and 2. The rate coefficients demonstrate no dependence on pressure or initial concentration of OH radicals within the experimental ranges. The observed pressure independence was anticipated, because the mechanisms of reactions 1–3 were expected to be those of atom abstraction (see next

TABLE 2: Conditions and Results of Experiments to Measure Rate Coefficients of the Reactions of Hydroxyl Radicals with Methane and Propane

			$OH + CH_4 \rightarrow H_2O + CH_3$ (2)			
no.[a]	T/K	P/kPa	$[CH_4]$ range/ 10^{15} molecule cm^{-3}	I^b/mJ pulse^{-1} cm^{-2}	$[OH]_0$/10^{10} molecule cm^{-3}	$k_2{}^c$/10^{-15} molecule^{-1} cm^3 s^{-1}
1	298	13.46	3.41–20.5	11	6.1	6.48 ± 0.19
2	298	13.43	3.51–20.7	3.6	2.0	6.29 ± 0.34
3	299	13.43	5.04–29.5	11	27	6.75 ± 0.12
4	299	13.43	5.11–29.9	4.1	10	6.78 ± 0.14
5	341	6.71	5.86–18.7	10	8.5	15.19 ± 0.57
6	341	6.71	6.05–19.1	2.6	2.2	15.22 ± 0.62
7	408	13.43	3.02–38.9	10	7.7	36.7 ± 1.2
8	408	13.43	3.00–38.1	4.3	3.3	37.1 ± 1.3
9	507	13.43	2.55–21.6	12	7.3	108.5 ± 3.7
10	507	13.43	2.56–21.7	3.3	2.0	106.9 ± 3.6
11*	606	24.15	2.05–12.5	13	2.5	243.7 ± 8.7
12	706	13.41	0.422–6.47	13	11	482 ± 12
13	706	13.41	0.427–6.41	3.3	2.9	481.9 ± 7.5
14*	807	13.43	0.121–4.00	14	3.2	803 ± 19
15*	908	13.41	0.271–2.70	11	16	1246 ± 42
16*	908	13.41	0.271–2.70	2.6	3.8	1232 ± 43
17*	961	6.71	0.333–1.260	13	6.3	1421 ± 43
18*	1009	21.46	0.230–1.33	11	12	1687 ± 72
19*	1009	21.46	0.236–1.33	3.6	3.8	1670 ± 62

			$OH + C_3H_8 \rightarrow$ products (3)			
no.[a]	T/K	P/kPa	$[C_3H_8]$ range/ 10^{14} molecule cm^{-3}	I^b/mJ pulse^{-1} cm^{-2}	$[OH]_0$/10^{10} molecule cm^{-3}	$k_3{}^c$/10^{-12} molecule^{-1} cm^3 s^{-1}
1*	296	12.07	3.78–20.3	8.6	1.0	1.083 ± 0.055
2	296	12.01	1.73–32.7	13	3.7	1.081 ± 0.024
3	339	12.09	3.28–33.5	13	6.7	1.487 ± 0.034
4	339	12.09	3.25–34.9	4.1	2.1	1.453 ± 0.044
5	407	6.71	1.86–18.0	12	2.1	2.156 ± 0.092
6	495	12.05	1.34–11.9	8.9	2.7	3.37 ± 0.15
7	605	6.71	1.17–4.69	4.8	2.4	4.91 ± 0.22
8	705	12.05	0.460–2.88	13	3.0	6.65 ± 0.20
9	765	6.68	0.453–4.39	14	7.7	7.41 ± 0.30
10	765	6.68	0.482–3.83	4.8	2.6	7.37 ± 0.38
11	805	24.13	0.498–3.65	13	2.7	8.37 ± 0.20
12*	908	12.05	0.429–4.00	12	15	10.23 ± 0.31
13*	908	12.05	0.408–4.12	2.9	3.6	10.36 ± 0.19

[a] Experiment number. $[N_2O] = 0$ was in experiments marked with *. [b] Photolysis laser intensity. [c] Error limits represent 2σ statistical uncertainties only. Maximum estimated systematic uncertainty is 5% of the rate coefficient value (see text).

section). The fact that the rate coefficients are independent of the initial OH radical concentration indicates an absence of any influence of potential secondary reactions on the kinetics of OH radicals, as can be expected by the low values of $[OH]_0$ (1.0×10^{10}–3.0×10^{11} molecule cm^{-3}) estimated as upper limits. Similarly, the observed absence of any correlation between the measured rate coefficients and the photolysis laser intensity indicates that the potential effects of reactions between OH and the products of the laser photolysis of molecular substrates are negligible. At the highest temperatures used in the study of reaction 1, the absence of any potential effects of thermal decomposition of molecular chlorine was verified by measuring rate coefficients at different pressures and bulk flow velocities varied by a factor of approximately 2.

Temperature dependence values of the bimolecular rate coefficients for reaction 1–3 are displayed in Figures 5 and 6 in Arrhenius coordinates. The rate coefficients exhibit positive temperature dependence that can be represented with the following modified three-parameter Arrhenius expressions
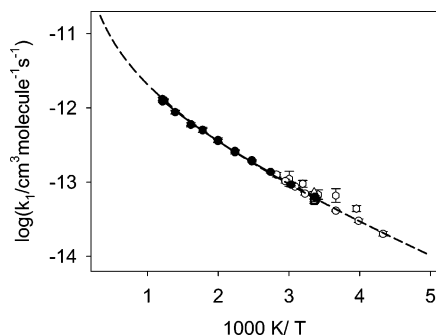
Figure 5. Temperature dependence of the rate coefficient for reaction 1 displayed in Arrhenius coordinates. Closed circles (●) represent the current experimental data; open square (□) represents ref 5; open triangle up (△) represents ref 6; open diamond (◇) represents ref 7; open hexagons (⬡) represent ref 8; open circles (○) represent ref 9. The solid line (−) represents the modified Arrhenius fit of eq III; the dashed line (- - -) represents eq VI (see text).
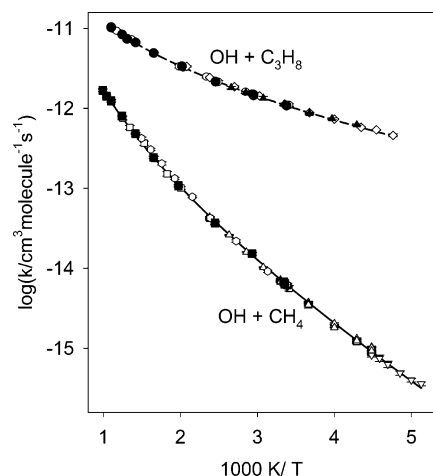

Figure 6. Temperature dependences of the rate coefficients for reactions 2 and 3 displayed in Arrhenius coordinates. Reaction 2: Closed squares (■) represent the current experimental data; open triangles up (△) represent ref 10; open squares (□) represent ref 11; open triangles down (▽) represent ref 12; open hexagons (⬡) represent ref 13; the solid line (−) represents the result of the fit of the current experimental data only (eq IV). Reaction 3: closed circles (●) represent the current experimental data; open circles (○) represent ref 14; closed triangles up (▲) represent ref 15; open diamonds (◇) represent ref 16; the dashed line (- - -) represents the result of the fit of the current experimental data only (eq V).

within their corresponding experimental temperature ranges

$$k_1 = 3.59 \times 10^{-16}\, T^{1.35} \exp(-745\ \mathrm{K}/T)\ \mathrm{cm^3\ molecule^{-1}\ s^{-1}}$$
$$(297-826\ \mathrm{K})\quad \mathrm{(III)}$$

$$k_2 = 3.82 \times 10^{-19}\, T^{2.38} \exp(-1136\ \mathrm{K}/T)\ \mathrm{cm^3\ molecule^{-1}\ s^{-1}}$$
$$(298-1009\ \mathrm{K})\quad \mathrm{(IV)}$$

$$k_3 = 6.64 \times 10^{-16}\, T^{1.46} \exp(-271\ \mathrm{K}/T)\ \mathrm{cm^3\ molecule^{-1}\ s^{-1}}$$
$$(296-908\ \mathrm{K})\quad \mathrm{(V)}$$

Maximum deviations of our experimental rate coefficient values from the rate coefficient values calculated using these parametrized expressions are 7.0% (expression III), 4.8% (expression IV), and 2.5% (expression V). Error limits of the parameters in expressions III−V are not reported, because these parameters bear no physical meaning.

The sources of error in the measured experimental physical parameters, such as total flow rate, flow rate of the molecular

substrate, ratios of the calibrated volumes, reaction pressure, temperature, time, and S_t and S_{sc} values, were subdivided into statistical and systematic categories according to their physical nature or the behavior observed during the performance of the experiments. The evaluation of potential systematic errors was mainly based on the finite accuracy of the equipment. The uncertainties in the measured experimental parameters were propagated to the final values of the uncertainties in the measured rate coefficients, using different mathematical procedures for propagating systematic and statistical uncertainties.[27] The error limits of the experimentally obtained rate coefficients listed in Tables 1 and 2 represent the 2σ level of statistical (random) uncertainty only. The evaluated maximum of the systematic uncertainty in the experimental rate coefficients is 5% of the value.

III. Potential Energy Surface and Transition-State Theory Model of Reaction 1

III. A. Potential Energy Surface Study. The potential energy surface (PES) of reaction 1, that of OH with Cl_2, was studied using quantum chemical approaches. Two methods were used for the optimization of molecular structures and calculation of vibrational frequencies: density functional BH&HLYP[28,29] and QCISD,[30] both with the aug-cc-pVDZ basis set.[31] The version of the BH&HLYP functional implemented in *Gaussian 98*[32] was used which, as described in the Gaussian manual, is different from that of ref 28. The sets of vibrational frequencies obtained using BH&HLYP and QCISD methods are similar to each other (Table 1S in the Supporting Information). The *Gaussian 98*[32] program was used in all PES calculations. In addition, high-level single-point energy calculations were carried out for the PES stationary points using the QCISD(T)[30] method with two basis sets, aug-cc-pVDZ and aug-cc-pVTZ.[31] All QCISD(T) results lead to the same qualitative conclusions regarding the mechanism of reaction 1; energy values quoted in the text henceforth are those obtained in the QCISD(T)/aug-cc-pVTZ//QCISD/aug-cc-pDTZ calculations and include vibrational zero-point energies unless stated otherwise. The results of the PES study are summarized in Table 3 and Figure 7, and the detailed information is given in the Supporting Information (Table 1S).

The reaction path leading from the OH + Cl_2 reactants to the HOCl + Cl products has an energy barrier (transition state TS1) and two shallow van der Waals minima on both the reactants (vdW1) and the products (vdW2) sides of the barrier (-6.5 relative to the reactants and -10.1 kJ mol^{-1} relative to the products). The energy barrier height was overestimated at both the BH&HLYP (39 kJ mol^{-1}) and the QCISD (29 kJ mol^{-1}) levels, as can be seen by comparing these values with the 11.6 kJ mol^{-1} experimental activation energy obtained if the experimental $k_1(T)$ dependence is fit with a two-parameter Arrhenius expression. The use of the higher-level QCISD(T) single-point calculations reduced the barrier height to more realistic values in the 11.1−16.6 kJ mol^{-1} range (see Table 3 for individual values corresponding to each combination of basis set and geometry optimization method).

An attempt was made to locate a transition state (PES saddle point) for the reaction channel leading from OH + Cl_2 to the HCl + ClO products. In these calculations, a two-dimensional PES scan (Cl−Cl and O−H, starting from the HOCl + Cl product valley) at the BH&HLYP/aug-cc-pVDZ level and three-dimensional scan (Cl−Cl, O−H, and O−Cl) at the B3LYP[29,33]/aug-cc-pVDZ level were performed. The searched-for transition

TABLE 3: Energies of Reactants, Products, and Stationary Points on the PES of Reaction 1 Obtained in Quantum Chemical Calculations[a]

method	species[b]							
	HOCl + Cl	HCl + ClO	vdW1	vdW2	vdW3	IP1	TS1	TS2
	BH&HLYP/aug-cc-pVDZ optimization							
BH&HLYP/aug-cc-pVDZ	15.11	−8.04	−5.63	5.80	−14.11	10.39	39.13	49.62
QCISD(T)/aug-cc-pVDZ	−8.17	−30.86	−7.30	−16.65	−33.87	−15.68	11.12	26.34
QCISD(T)/aug-cc-pVTZ	4.45	−26.50	−6.18	−6.70	−29.58	−3.19	13.91	44.55
	QCISD/aug-cc-pVDZ optimization							
QCISD/aug-cc-pVDZ	−6.87	−27.62	−6.44	−14.41	−37.12	−13.44	29.22	34.53
QCISD(T)/aug-cc-pVDZ	−9.52	−30.05	−7.50	−18.80	−41.13	−17.08	13.85	30.69
QCISD(T)/aug-cc-pVTZ	3.51	−24.40	−6.47	−6.61	−34.48	−4.20	16.55	31.67
experimental[c]	9.7 ± 3.3	−29.2 ± 3.5					9.63	

[a] Energy values are given in kJ mol^{-1} relative to OH + Cl$_2$ and include zero-point vibrational energy (ZPE). [b] See text for the description of the individual PES stationary points. [c] Ref 35 for products ($\Delta H_0°$) and the result of transition-state theory fit of experimental $k_1(T)$ dependence for TS1.
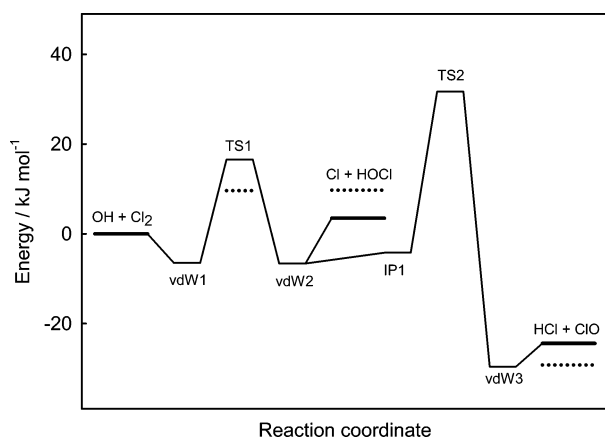

Figure 7. Potential energy surface of reaction 1 obtained in quantum chemical calculations (see text). QCISD(T)/aug-cc-pVTZ//QCISD/aug-cc-pDTZ energies are used for the plot (solid horizontal lines, −). Dotted lines (···) indicate the experimental values of $\Delta H_0°$ for HOCl + Cl and HCl + ClO (ref 35) and the energy barrier height for TS1 obtained in transition-state theory modeling of the experimental data.

state could not be found. The three-dimensional scan produced a PES ridge without a saddle point separating the OH + Cl$_2$ and the HCl + ClO valleys.

However, a reaction path leading from the van der Waals complex corresponding to the HOCl + Cl products (vdW2) to HCl + ClO was found using both the BH&HLYP and QCISD geometry optimizations. This path leads from vdW2 through the structure denoted as IP1, a transition state TS2, and a van der Waals complex vdW3 corresponding to the HCl + ClO products. The IP1 structure (Table 1S in the Supporting Information) has energy that is 7.7 kJ mol^{-1} below that of HOCl + Cl and resembles another shallow-well van der Waals complex. The molecular structure optimization procedure implemented in *Gaussian 98*[32] reported IP1 as a PES minimum; however, a BH&HLYP-level scan of the Cl−Cl distance leading from IP1 to vdW2 indicated that the path between these two structures is barrierless. Therefore, it is likely that IP1 represents an inflection point on the reaction PES, not a local minimum.

The TS1 PES saddle point represents the dynamic bottleneck of the OH + Cl$_2$ → HOCl + Cl reaction. Any further chemical transformation of the exit van der Waals complex (vdW2) can be expected to largely favor dissociation into HOCl + Cl via a very loose[34] transition state with densities of states that are much larger than those of the tighter PES saddle points TS1 and TS2. In addition, the energy of the transition state for the pathway leading to the HCl + ClO products (TS2) is higher than that of the HOCl + Cl products by 28.2 kJ mol^{-1}, indicating that the

potential formation of the HCl + ClO products can be neglected in the OH + Cl$_2$ reaction.

III. B. Rate Coefficient Calculations. To provide means for an extrapolation of the experimental $k_1(T)$ dependence to temperatures outside the experimental range, a transition-state theory model of reaction 1 was created in the current work. In the initial approximation to the properties of the reaction transition state, geometry, and vibrational frequencies obtained at the QCISD/aug-cc-pVDZ level, calculations were used together with the experimental properties of the reactants and products.[35] Rate coefficient values were calculated using the classical transition-state theory formula (see, for example, ref 36).

The reaction transition state has one torsional degree of freedom. The PES of this torsion, obtained using a relaxed scan of the H−O−Cl−Cl dihedral angle has two unequal maxima (7.5 and 28.1 kJ mol^{-1}). In the rate constant calculations, the partition function of this torsional degree of freedom was calculated by summing over the energy levels evaluated via a numerical solution of the Schrödinger equation. The *FGH1D* program[37] of Johnson was used in the energy level calculations. Existence of the low-lying excited electronic states[35] of OH (139.7 cm^{-1}) and Cl (882.5 cm^{-1}) was taken into account in the rate coefficient calculations.

The energy barrier of reaction 1 was adjusted to provide a match with the experimental $k_1(T)$ dependence. A combined set of data formed by the results of the current study and those of Gilles et al.[9] (included to represent the low-temperature $k_1(T)$ dependence) was used in the fitting. The resultant model reproduces the experimental $k_1(T)$ dependence very well, with the calculated room-temperature preexponential factor differing from the experimental one by a factor of 1.4. An adjustment of the lowest vibrational frequency of the transition state (from 171 to 242 cm^{-1}) brought the calculated temperature dependence into agreement with the experimental one. The final adjusted value of the reaction energy barrier is 9.6 kJ mol^{-1}.

The rate coefficient values extrapolated via modeling can be represented by the modified Arrhenius expression

$$k_1 = 1.35 \times 10^{-16} T^{1.50} \exp(-723 \text{ K}/T) \text{ cm}^3 \text{ molecule}^{-1} \text{ s}^{-1}$$

$$(200-3000 \text{ K}) \quad \text{(VI)}$$

with deviations from the calculated values of less than 4% between 200 and 3000 K.

Information on reaction 1 obtained in the current work can be used in combination with the known thermochemistry to derive the temperature dependences of the rate coefficient of

Gas-Phase Reactions of OH

J. Phys. Chem. A, Vol. 108, No. 47, 2004 **10471**

the reverse process, that of the reactions of abstraction of a chlorine atom from HOCl by Cl:

$$Cl + HOCl \rightarrow OH + Cl_2 \quad (-1)$$
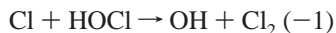
The transition-state theory model of reaction 1 created in the current study results in the $k_{-1}(T)$ dependence that can be represented by the expression

$$k_{-1} = 2.76 \times 10^{-16} T^{1.39} \exp(177 \text{ K}/T) \text{ cm}^3 \text{ molecule}^{-1} \text{ s}^{-1}$$
$$(200-3000 \text{ K}) \quad (VII)$$

with deviations from the calculated values of less than 7%.

Here, thermochemical properties from ref 35 were used. The uncertainty in expression VII originates, primarily, from that in the enthalpy of reaction 1. The uncertainty factor can be calculated for any temperature using the van't Hoff factor with the cumulative reaction enthalpy uncertainty of 3.3 kJ mol^{-1}. The bimolecular rate coefficient values for reaction -1 calculated from the temperature dependence of expression VII are consistent with the recommendation given in ref 38 for Cl + HOCl $\rightarrow$ products within reported uncertainties in a common temperature interval.

IV. Discussion

Reactions 2 and 3 have been studied in the present work to validate the experimental apparatus employed for the first time after its construction. Hydrogen atom abstraction from hydrocarbons by hydroxyl radicals plays a fundamental role in the chemistry of atmospheric and combustion processes; for this reason, reactions 2 and 3 had been extensively studied previously. These earlier results are in general agreement with each other. Reviews of these data can be found in ref 13 for reaction 2 and in ref 16 for reaction 3, and they are not repeated here. The rate coefficients obtained in the current study are in agreement with these earlier measurements (see Figure 6; data are exemplified by refs 10−13 and 14−16 for reactions 2 and 3, respectively). For example, over common temperature ranges, the maximum deviations between the rate coefficient values calculated using modified three-parameter Arrhenius expressions IV and V and those calculated using the expressions recommended in refs 11 and 12 for reaction 2 and in refs 14 and 15 for reaction 3 are the following: 5.4% and 2.5% for reaction 2 and 5.1% and 1.3% (of the average rate coefficient value) for reaction 3. Such a good agreement with previously obtained data gives us confidence in the measurements performed with the experimental apparatus employed in this work.

All previous studies of the reaction of OH + Cl$_2$ have been performed at low temperatures (see Figure 5). Data reported in refs 5−7 were measured at room temperature only, and they are in agreement with our data obtained at room temperature within experimental errors. Experimental temperature-dependent kinetic investigations of reaction 1 were carried out in two works.[8,9] Our data are in agreement with both of these studies over the common temperature ranges, within reported experimental errors. Nevertheless, only data from ref 9 were included to represent the low-temperature $k_1(T)$ dependence for the purposes of rate coefficient modeling. This preference was given to the results of ref 9 because of the wider temperature range used, better purity of molecular chlorine sample, and experimental conditions free from potential contributions of the OH heterogeneous reactions.

The theoretical simulation of reaction 1 was performed in this work to assess possible reaction pathways and to provide means for the extrapolation of the $k_1(T)$ temperature dependence to outside the experimental temperature range. The PES of reaction 1 obtained in quantum chemical calculations demonstrates good agreement with experimental results. The vibrational frequencies of the transition state (TS1) obtained at both the BH&HLYP and QCISD levels yield realistic preexponential factors; only a minor adjustment (see section III. B.) was needed to bring the model to complete agreement with the experimental $k_1(T)$ dependence. The QCISD(T)/aug-cc-pVTZ level energy calculations also provide reasonable agreement with the experimental values of the reaction enthalpy and barrier height, with deviations of 5−6 and 4−7 kJ mol^{-1}, respectively (see Table 3). Theoretical model predictions suggest OH + Cl$_2$ $\rightarrow$ HOCl + Cl as the main channel for reaction 1, in agreement with the room-temperature evaluation of the branching ratio for the OH reaction with Cl$_2$ presented in the work of Loewenstein et al.[7] The agreement between experimental and computational results provides support for further use of the computational techniques applied here for the treatment of other reactions of similar types.

Supporting Information Available: Supplement including the results of the quantum chemical calculations (Table 1S). This material is available free of charge via the Internet at http://pubs.acs.org.

References and Notes

(1) Chang, W.-D.; Senkan, S. M. *Environ. Sci. Technol.* **1989**, *23*, 442.

(2) Procaccini, C.; Bozzelli, J. W.; Longwell, J. P.; Smith, K. A.; Sarofim, A. F. *Environ. Sci. Technol.* **2000**, *34*, 4565.

(3) Procaccini, C.; Bozzelli, J. W.; Longwell, J. P.; Sarofim, A. F.; Smith, K. A. *Environ. Sci. Technol.* **2003**, *37*, 1684.

(4) Aizava, T.: Kamimoto, T.; Tamaru, T. *Appl. Opt.* **1999**, *38*, 1733.

(5) Leu, M. T.; Lin, C. L. *Geophys. Res. Lett.* **1979**, *6*, 425.

(6) Ravishankara, A. R.; Eisele, F. L.; Wine, P. H. *J. Chem. Phys.* **1983**, *78*, 1140.

(7) Loewenstein, L. M.; Anderson, J. G. *J. Phys. Chem.* **1984**, *88*, 6277.

(8) Boodaghians, R. B.; Hall, I. W.; Wayne, R. P. *J. Chem. Soc., Faraday Trans.* 2 **1987**, *83*, 529.

(9) Gilles, M. K.; Burkholder, J. B.; Ravishankara, A. R. *Int. J. Chem. Kinet.* **1999**, *31*, 417.

(10) Vaghjiani, G. L.; Ravishankara, A. R. *Nature (London)* **1991**, *350*, 406.

(11) Dunlop, J. R.; Tully, F. P. *J. Phys. Chem.* **1993**, *97*, 11148.

(12) Gierczak, T.; Talukdar, R. K.; Herndon, S. C.; Vaghjiani, G. L.; Ravishankara, A. R. *J. Phys. Chem. A* **1997**, *101*, 3125.

(13) Bonard, A.; Daele, V.; Delfau, J.-L.; Vovelle, C. *J. Phys. Chem. A* **2002**, *106*, 4384.

(14) Droege, A. T.; Tully, F. P. *J. Phys. Chem.* **1986**, *90*, 1949.

(15) Talukdar, R. K.; Mellouki, A.; Gierczak, T.; Barone, S.; Chiang, S.-Y.; Ravishankara, A. R. *Int. J. Chem. Kinet.* **1994**, *26*, 973.

(16) Kozlov, S. N.; Orkin, V. L.; Huie, R. E.; Kurylo, M. J. *J. Phys. Chem. A* **2003**, *107*, 1333.

(17) Taylor, P. H.; D'Angelo, J. A.; Martin, M. C.; Kasner, J. H.; Dellinger, B. *Int. J. Chem. Kinet.* **1989**, *21*, 829.

(18) Atkinson, R.; Baulch, D. L.; Cox, R. A.; Hampson, R. F., Jr.; Kerr, J. A.; Rossi, M. J.; Troe, J. *J. Phys. Chem. Ref. Data* **1997**, *26*, 1329.

(19) Wollenhaupt, M.; Carl, S. A.; Horowitz, A.; Crowley, J. N. *J. Phys. Chem. A* **2000**, *104*, 2695.

(20) D'Ottone, L.; Campuzano-Jost, P.; Bauer, D.; Hynes, A. J. *J. Phys. Chem. A* **2001**, *105*, 10538.

(21) Okabe, H. *Photochemistry of Small Molecules*; Wiley: New York, 1978.

(22) Silvente, E.; Richter, A. C.; Hynes, A. J. *J. Chem. Soc., Faraday Trans.* **1997**, *93*, 2821.

(23) Tully, F. P.; Golgsmith, J. E. M. *Chem. Phys. Lett.* **1985**, *116*, 345.

(24) Tully, F. P.; Droege, A. T.; Koszykowski, M. L.; Melius, C. F. *J. Chem. Phys.* **1986**, *90*, 691.

(25) Orkin, V. L.; Huie, R. E.; Kurylo, M. J. *J. Phys. Chem.* **1996**, *100*, 8907.

(26) Kurylo, M. J.; Orkin, V. L. *Chem. Rev.* **2003**, *103*, 5049.

(27) Bevington, P. R. *Data Reduction and Error Analysis for the Physical Sciences*; McGraw-Hill: New York, 1969.

(28) Becke, A. D. *J. Chem. Phys.* **1993**, *98*, 1372.

(29) Lee, C. T.; Yang, W. T.; Parr, R. G. *Phys. Rev. B* **1988**, *37*, 785.

(30) Pople, J. A.; Head-Gordon, M.; Raghavachari, K. *J. Chem. Phys.* **1987**, *87*, 5968.

(31) Kendall, R. A.; Dunning, T. H., Jr.; Harrison, R. J. *J. Chem. Phys.* **1992**, *96*, 6796.

(32) Frisch, M. J.; Trucks, G. W.; Schlegel, H. B.; Scuseria, G. E.; Robb, M. A.; Cheeseman, J. R.; Zakrzewski, V. G.; Montgomery, J. A., Jr.; Stratmann, R. E.; Burant, J. C.; Dapprich, S.; Millam, J. M.; Daniels, A. D.; Kudin, K. N.; Strain, M. C.; Farkas, O.; Tomasi, J.; Barone, V.; Cossi, M.; Cammi, R.; Mennucci, B.; Pomelli, C.; Adamo, C.; Clifford, S.; Ochterski, J.; Petersson, G. A.; Ayala, P. Y.; Cui, Q.; Morokuma, K.; Malick, D. K.; Rabuck, A. D.; Raghavachari, K.; Foresman, J. B.; Cioslowski, J.; Ortiz, J. V.; Stefanov, B. B.; Liu, G.; Liashenko, A.; Piskorz, P.; Komaromi, I.; Gomperts, R.; Martin, R. L.; Fox, D. J.; Keith, T.; Al-Laham, M. A.; Peng, C. Y.; Nanayakkara, A.; Gonzalez, C.; Challacombe, M.; Gill, P. M. W.; Johnson, B. G.; Chen, W.; Wong, M. W.; Andres, J. L.; Head-Gordon, M.; Replogle, E. S.; Pople, J. A. *Gaussian 98*, revision A.7; Gaussian, Inc.: Pittsburgh, PA, 1998.

(33) Becke, A. D. *J. Chem. Phys.* **1993**, *98*, 5648.

(34) Benson, S. W. *Thermochemical Kinetics,* 2nd ed.; John Wiley and Sons: New York, 1976.

(35) Chase, M. W., Jr. *J. Phys. Chem. Ref. Data* **1998**, Monograph 9.

(36) Johnston, H. S. *Gas-Phase Reaction Rate Theory*; The Ronald Press: New York, 1966.

(37) Johnson, R. D. I. *FGH1D,* a PC/Windows program for computing vibrational levels for nonharmonic potentials; National Institute of Standards and Technology: Gaithersburg, MD 20899.

(38) DeMore, W. B.; Sander, S. P.; Golden, D. M.; Hampson, R. F.; Kurylo, M. J.; Howard, C. J.; Ravishankara, A. R.; Kolb, C. E.; Molina, M. J. *JPL Publ.* **1997**, *4*, 29.